Research Article | Vol. 29, No. 15 / 19 July 2021 / Optics Express 23461
Optics EXPRESS

Classification of atmospheric aerosols and clouds by use of dual-polarization lidar measurements

SIQI QI,[1,2] ZHONGWEI HUANG,[1,*] XIAOJUN MA,[2,3] JIANPING HUANG,[1] TIAN ZHOU,[1] SHUANG ZHANG,[1] QINGQING DONG,[1] JIANRONG BI,[1] AND JINSEN SHI[1]

[1]*Collaborative Innovation Center for West Ecological Safety (CIWES), College of Atmospheric Sciences, Lanzhou University, Lanzhou, 73000, China*
[2]*Department of Atmospheric and Oceanic Sciences & Institute of Atmospheric Sciences, Fudan University, Shanghai, 200438, China*
[3]*Innovation Center of Ocean-Atmosphere System Observation and Prediction, Zhuhai Fudan Innovation Institute, Hengqin New Area, Zhuhai, Guangdong, China*
[*]*huangzhongwei@lzu.edu.cn*

Abstract: Accurate identification of aerosols and cloud from remote sensing observations is of importance for quantitatively evaluating their radiative forcing and related impacts. Even though polarization lidar has exhibited a unique advantage of classifying atmospheric aerosols and clouds over the past several decades, polarization measurements are often achieved at one wavelength (UV or VIS) using laser remote sensing. To better identify the types of aerosols and clouds, we developed a ground-based dual-polarization lidar system that can simultaneously detect polarization measurements at wavelengths of 355 nm and 532 nm. Our results show that the volume depolarization ratios (VDRs) at 355 nm and 532 nm markedly differ for typical types of aerosols and clouds in the atmosphere. For non-spherical particles, the ratio of VDRs at 532 nm and 355 nm are 2.87 ± 1.35 for ice cloud and 1.51 ± 0.29 for dust-dominated aerosols, respectively. However, for spherical particles, the ratios are 0.43 ± 0.26 for water cloud and 0.56 ± 0.05 for air pollutants. Consequently, we proposed a simple reliable method for classifying atmospheric aerosols and clouds from polarization measurements observed by the developed lidar system. The proposed method first distinguishes clouds from aerosols using a combination of the color ratio (CR, 532 nm/355 nm) and attenuated backscattering coefficients (ABC) at 532 nm. Then, subtypes of clouds and aerosols are identified based on the ratio of VDRs at 532 nm and 355 nm. The results showed that dual-polarization lidar measurements can remarkably improve the classification of atmospheric aerosols and clouds, compared with results using a traditional method. This study illustrates that more information on atmospheric aerosols and clouds can be obtained from polarization measurements at multiple wavelengths by active remote sensing.

1. Introduction

Previous studies have shown that aerosols and clouds play a significant role in regional and global climate systems [1]. Aerosols can change the radiation balance of Earth's atmospheric system by scattering and absorbing shortwave and longwave radiation [2–5]. In addition, aerosols can act as cloud condensation nuclei, consequently affecting the cloud occurrence and lifetime [6–9] and changing the microphysics of clouds [10,11], which is related to the number, phase and size of cloud droplets and ice crystals [12,13]. Clouds also have a strong modulation effect on Earth's radiation budget by reflecting solar radiation and absorbing longwave thermal emission from Earth. For example, the net effect of boundary layer clouds is cooling the climate system

#430456 https://doi.org/10.1364/OE.430456
Journal © 2021 Received 10 May 2021; revised 26 Jun 2021; accepted 26 Jun 2021; published 9 Jul 2021

Optics EXPRESS

[14,15]. On the other hand, various aerosols, which mainly come from natural and anthropogenic pollution processes, play different roles in the atmosphere. It has been proven that anthropogenic aerosols can completely change the attribution of drought to meteorological variables by causing large negative anomalies of surface temperature [16,17], effective energy and precipitation [18], and also favor haze conditions in particular periods of the year [19].

The influence of aerosols on atmospheric radiation depends on the spatial-temporal distribution of their microphysical and chemical properties. In recent years, ground-based and spaceborne lidar has been widely used in aerosol and cloud detection [20,21,22–29,30]. Reichardt et al. [31] developed a Raman lidar for unattended, continuous multi-parameter atmospheric profile measurements, which is used to observe water vapor, temperature, aerosols and clouds in the atmosphere. Intrieri et al. [32]. determined the temporal distributions of cloudiness, the vertical distribution of cloud boundary heights and the occurrence of the liquid phase in the clouds with a combination of radar/lidar observations. Li et al. [33] analyzed the long-term variation in the cloud droplet number concentrations (N_d) from space-based lidar measurements, indicating that the climatology of temperature-dependent N_d can reduce the uncertainties of indirect effect estimations of aerosols in model simulations. Yorks et al. [34] analyzed the optical property trends of ice clouds and liquid water clouds (altocumulus clouds) based on four-year observations from a multi-wavelength polarization lidar. Ansmann et al. [35] studied several pollution outbreaks in Europe during the Second Aerosol Characterization Experiment (ACE 2) in the summer of 1997 based on multi-wavelength lidar and sun photometer measurements. Tesche et al. [36]. investigated the vertical distributions of Sahara dust in southern Morocco by using Raman lidar and high-spectral-resolution lidar (HSRL). Using a combination of lidar measurements of dust aerosols during three field activities, Zhou et al. [37] found that the frequency of dust occurrence in Northwest China was higher than 88%, and the maximum height of dust layers typically reached 7.8–9 km or higher. Moreover, numerous previous studies have focused on lidar measurements of the vertical distributions of aerosols and clouds in China [38–44]. Hu et al. [45] observed the characterization of Taklimakan dust (including polluted dust) in Kashi using multi-wavelength polarization Raman lidar in April 2019. Sugimoto et al. [46] observed fluorescence signals from dust aerosols and air pollutants in the atmosphere using a lidar spectrometer with excitation wavelength of 355 nm. With the development of space technology, increasing attention has been paid to spaceborne lidar in global aerosol research due to its advantages of a wide detection range and high resolution [47,48]. More frequent summer dust aerosol plumes over the Tibetan Plateau have been detected by the Cloud–Aerosol Lidar and Infrared Pathfinder Satellite Observations (CALIPSO) lidar, showing that these dust eruptions will affect the radiation balance of the atmosphere in the region [49]. Moreover, the vertical distribution of aerosols and clouds in the atmosphere has been studied using four-year CALIPSO observations in the Arctic [50].

Classification of aerosols and clouds is the basis for investigating their effects on climate systems and the environment. In recent decades, polarization lidar measurements have been widely used to identify different aerosol and cloud types [51–58]. Many methods have been proposed to classify and identify aerosols [59–61] and clouds [62–64]. Polarization lidar has unique research capabilities in unambiguous cloud-phase discrimination and an almost ideal sensitivity to cirrus clouds [65]. Liu et al. [66] introduced a three-dimensional algorithm for distinguishing clouds and aerosols detected in a two-wavelength backscatter lidar profile by using the layer-averaged attenuation backscatter at 532 nm, the layer-averaged color ratio (1064 nm/532 nm), and the middle layer height from the CALIPSO observation mission, consequently improving the theoretical basis of the CALIPSO lidar cloud and aerosol discrimination (CAD) algorithm [67]. Zhou et al. [68] identified dust aerosols by using the depolarization–attenuated backscatter relationship from CALIPSO lidar observations. Wang and Sassen [69] distinguished various atmospheric targets, such as ice and water clouds, virga, precipitation, and aerosols, based

Optics EXPRESS

on lidar measurements. Zhao et al. [70] proposed a new algorithm for aerosol and cloud detection based on micro pulse lidar measurements. Veselovskii et al. [71] asserted that the calculation the accuracy of microphysical parameters of bimodal particle size distribution from multi-wavelength Mie-Raman lidar can reach 50%. Groß et al. [72] proposed that the combination of the lidar ratio and particle linear depolarization ratio can be used to distinguish continental pollution aerosols from other types of aerosols over Europe. Floutsi et al. [73] combined multi-wavelength polarization Raman lidar observations with HYSPLIT backward trajectory analysis to identify advection of biomass burning aerosols towards Punta Arenas. Burton et al. [74] identified aerosol types by integrating the lidar ratio, backscatter color ratio and depolarization ratio from lidar measurements. Moreover, the spectrum depolarization ratio of particles has also been reported in the literature by Burton et al. [75]. For dust-dominated aerosols, the DR at 532 nm is greater than that at 355 nm, but for smoke particles, the results are opposite [76]. Mishchenko et al. [77] found that the linear depolarization ratio (LDR) measurement of spectral backscatter can indicate the presence of smoke particles with complex morphology.

To better identify the types of aerosols and clouds, we developed a ground-based dual-polarization lidar system that can simultaneously detect polarization measurements at both 355 nm and 532 nm. In this study, a simple yet reliable method was proposed to distinguish the different types of aerosols and clouds from dual-polarization lidar measurements. In Section 2, the developed lidar system is briefly introduced. The results and discussion are provided in Section 3. Finally, the conclusion is given in Section 4.

2. Lidar and observational data

A ground-based dual-polarization lidar system that simultaneously collected polarization measurements at 532 nm and 355 nm was developed by Lanzhou University. A schematic diagram of the developed lidar system is shown in Fig. 1. The system employs a flash-lamp-pumped Nd:YAG laser to generate fundamental laser beam at wavelength of 1064 nm, then convert into a 532 nm source in second harmonic generation (SHG). Finally, 355 nm laser is generated combing the remaining 1064 nm and newly created 532 nm lasers in third harmonic generation (THG). After that the lidar system sends laser beams to the atmosphere simultaneously at wavelengths of 532 nm and 355 nm. The energy of a single pulse is ~ 210 mJ (532 nm) and ~80 mJ (355 nm), and the pulse repetition rate and duration are 20 Hz and 8.7 ns, respectively. Then, backscatter signals from atmospheric aerosols and clouds were collected by a receiving Schmidt-Cassegrain telescope with a diameter of 350 mm, consequently separated by a dichroic mirror. The field of view (FOV) of the system was 0.5 mrad. Polarization measurements at 532 nm and 355 nm were detected simultaneously by using two polarizing beam splitters (PBS). Finally, signals in analog and photon counting modes were simultaneously measured by Licel transient recorders and then detected by four photomultiplier tubes (PMTs). The spatial resolution and temporal resolution of the developed dual-polarization lidar system were 3.75 m and 2 min, respectively.

The vertical structure of tropospheric aerosols and clouds was measured by the developed lidar over northern China in Lanzhou (36.05 °N, 103.85 °E, 1493.1 m AGL) in March 2014 and Linze (34.73 °N, 114.00 °E) in April 2014. The volume depolarization ratio (VDR) is defined by the ratio of the parallel and perpendicular components of the backscattering signals, and the color ratio (CR (532/355)) is defined by the ratio of the attenuated backscattering coefficients (ABC) at 532 nm and 355 nm. Lidar data corrections, such as background subtraction, range correction and polarization calibration, were achieved in this study.

The VDR is the total depolarization ratio of atmospheric molecules and particles, whose value can be used to measure the physical properties of particles. It is a parameter of particle shape:

$$\delta = C\frac{\beta_{\perp}}{\beta_{//}}, \tag{1}$$

Optics EXPRESS

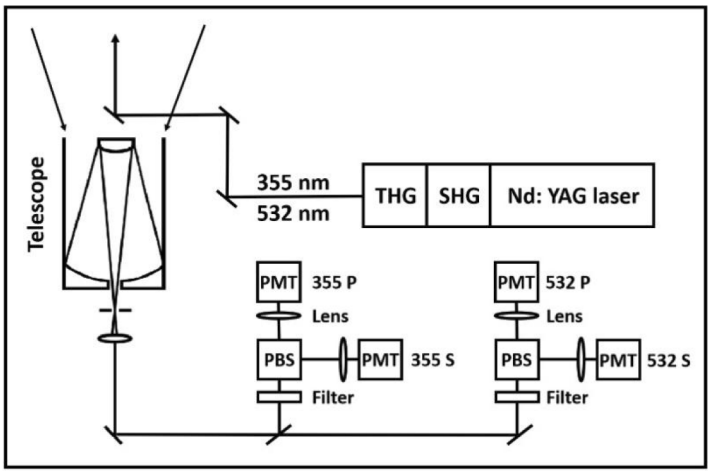

Fig. 1. Schematic diagram of the developed dual-polarization lidar system used in this study.

where $\beta_{\perp}$ is the attenuated backscattering coefficient of the perpendicular channel and $\beta_{//}$ is the attenuated backscattering coefficient of the parallel channel signal. C is the calibration factor of polarization measurements. In this study, the ratio of VDRs ($\delta_{532}/\delta_{355}$) is defined as a parameter to distinguish aerosols and clouds.

Color ratio is a parameter relating to particle size, in which large color ratios corresponds to coarse particle:

$$\chi = \frac{\beta_{532,\perp} + \beta_{532,//}}{\beta_{355,\perp} + \beta_{355,//}}. \tag{2}$$

3. Results and discussion

Dust events originating from the Taklimakan Desert and Gobi Desert usually occur in East Asia in late winter and spring. In March, 2014, there were dust-dominated aerosol events and haze episodes in Lanzhou, China. Figure 2 shows the vertical structure of clouds and aerosols observed by the developed dual-polarization lidar on March 5–6 and March 26–27. The results show that there was a distinct air pollutant layer at 0–2 km in the afternoon on March 5–6. The ABCs of the air pollutant layer were small with a low VDR (~0.1) at 532 nm. However, the VDRs at 532 nm were much smaller than those at 355 nm in this layer. On March 26–27, we found a dust layer at 0–2 km. The ABCs of the dust layer were small with a high VDR (~0.24) at 532 nm. However, the VDRs at 355 nm were much smaller than those at 532 nm in this layer. This phenomenon has been proven by other previous studies [75–77]. We also observed ice cloud layers at approximately 6–9 km on March 5–6. For ice clouds, at 532 nm, the ABCs were stronger and the VDRs were larger than the corresponding values of dust-dominated aerosols. However, it is interesting that the VDRs at 355 nm were smaller than those at 532 nm, also indicating similar results for ice clouds on other observed days in March and April. In addition, for water clouds, the VDRs at 355 nm were larger than those at 532 nm. Therefore, we can confirm that aerosols and clouds show different features on lidar measurements at UV and visible wavelengths, which may be related to particle size.

To explore the differences in aerosol and cloud observation results at 532 nm and 355 nm, we studied the relationship between the ABC, VDR and CR at wavelengths of 532 nm and 355 nm for typical types of aerosols and clouds, such as air pollutants (A), dust-dominated aerosols(D), water clouds (W), mixed phase clouds (MP) and ice clouds (I). Data sets of the five types were

Optics EXPRESS

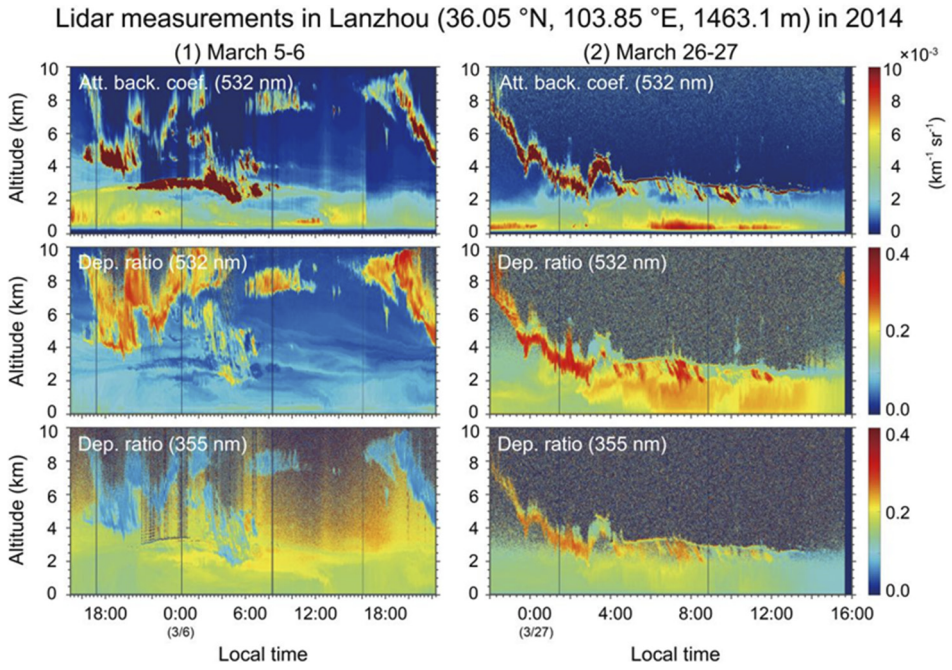

Fig. 2. Vertical structure of atmospheric aerosols and clouds observed by the developed lidar in Lanzhou (36.05°N, 103.85°E, 1493.1 m) on March 5–6 and March 26–27, 2014.

selected from polarization lidar measurements in March and April. The time and heights of the aerosol and cloud layers are summarized in Table 1. The relationships between the ABC and VDR at wavelengths of 532 nm and 355 nm for these five types are shown in Fig. 3. The results show that for ice clouds and dust-dominated aerosols, the VDRs at 532 nm were larger than 0.18, but those at 355 nm were smaller. Moreover, the VDR of ice cloud was the largest (smallest) at 532 (355) nm. In particular, the VDRs of water clouds and air pollutants were similar at both 532 nm and 355 nm, indicating that the VDR cannot be used to distinguish water clouds from air pollutants. In addition, classification of the four types cannot be achieved according to the results of the ABCs at 532 nm and 355 nm, even though they are slightly different.

The relationships between the CR (532/355), ABC and VDR at wavelengths of 532 nm and 355 nm for these five types are shown in Fig. 4. The CRs of ice clouds were the largest among the five types. According to the results, the relationships between the CR (532/355) and VDR at wavelengths of 532 nm and 355 nm did not show clear features for the four types. The combination of CRs and the ABC at the wavelength of 532 nm can distinguish atmospheric aerosols from clouds. The CRs of clouds are greater than 3.0, and the ABC at 532 nm is larger than 0.015/km/sr. These thresholds could be used to successfully separate clouds and aerosols. Finally, we compared the differences in VDRs at 532 nm and 355 nm for aerosols and clouds, as shown in Fig. 5. The VDRs of non-spherical particles (ice clouds and dust-dominated aerosols) at 532 nm are larger than those at 355 nm, but for spherical particles (water clouds and air pollutants), the opposite is true.

The mean values and standard deviations of the VDRs for the five types were calculated and are provided in Fig. 6. We can see that for aerosols, the average VDR values at 532 nm are 0.22 ± 0.02 for dust-dominated aerosols and 0.09 ± 0.01 for air pollutants, but these values are 0.16 ± 0.04 for dust-dominated aerosols and 0.17 ± 0.01 for air pollutants at 355 nm. In addition, for clouds, the average VDR values at 532 nm are 0.30 ± 0.07 (ice cloud), 0.05 ± 0.03

Optics EXPRESS

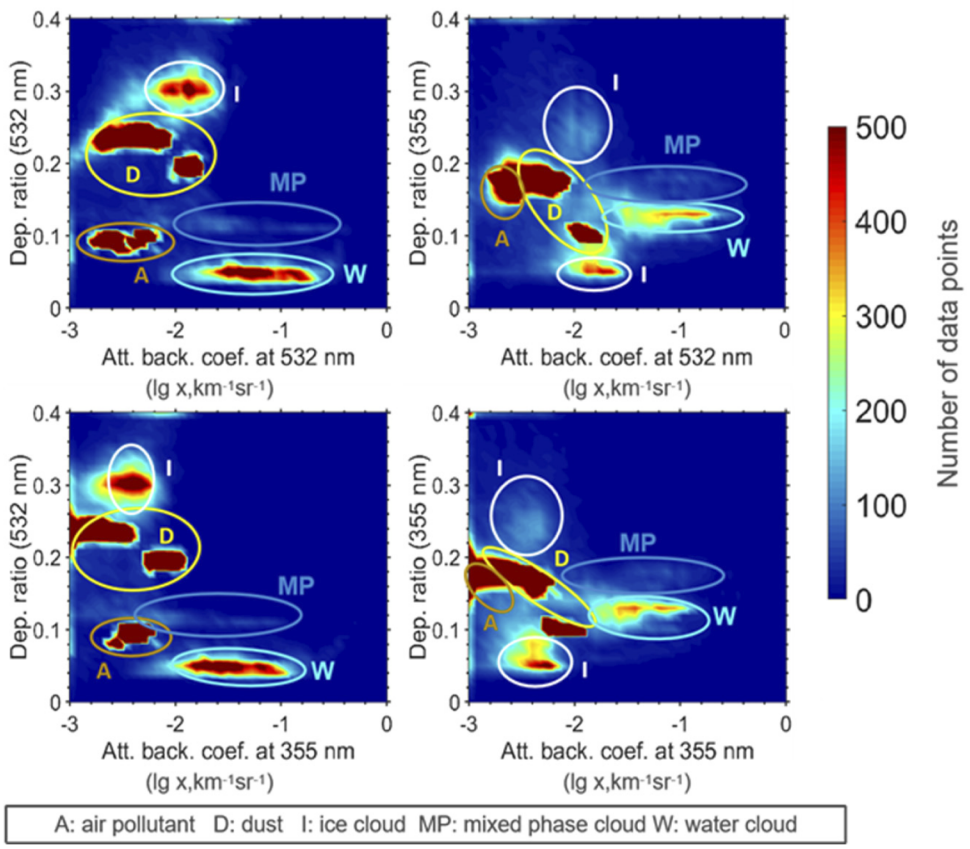

Fig. 3. Relationship between the attenuated backscatter coefficient and volume depolarization ratio at wavelengths of 532 nm and 355 nm for air pollutants (A), dust-dominated aerosols (D), ice clouds (I), water clouds (W) and mixed phase clouds (MP) from lidar measurements in Lanzhou in March and in Linze in April, 2014. The datasets are summarized in Table 1. The grid resolution is 40×40.

(water cloud) and 0.12 ± 0.05 (mixed phase cloud), while these values are 0.16 ± 0.12 (ice cloud), 0.13 ± 0.04 (water cloud) and 0.14 ± 0.07 (mixed phase cloud) at 355 nm. Then, we found that for non-spherical particles, the ratio of VDRs at 532 nm and 355 nm are 2.87 ± 1.35 for ice cloud and 1.51 ± 0.29 for dust-dominated aerosol, while for spherical particles, the ratios are 0.43 ± 0.26 for water cloud and 0.56 ± 0.05 for air pollutants. Finally, lidar observations of atmospheric aerosols and clouds in March and April were used to calculate the ratio of VDRs at 532 nm and 355 nm, as shown in Fig. 7 and 8. We found that layers of ice clouds and dust-dominated aerosols are clearly seen and separated from others. This study indicated that spectral VDRs at UV and visible wavelengths are very useful for the identification of aerosols and clouds in the atmosphere by lidar measurements.

Now, we can conclude that for spherical particles, the ratio of VDRs at 532 nm and 355 nm ($\delta_{532}/\delta_{355}$) are less than 1, while for non-spherical particles, the values are greater than 1. Moreover, we found that the threshold value of the ratio for dust-dominated aerosols is 1.1–2.5, and for air pollutants, this value is less than 0.8. According to this result, a ratio between 0.8 and 1.1 is attributed to a mixture of dust and air pollutants. These thresholds are consistent with our previous results (Huang et al., 2020). In addition, the ratio of VDRs for water clouds are less

Optics EXPRESS

Table 1. Information on the data points selected for the analysis shown in Figures 3–5.

Date (Location)	Ice cloud (I)	Water cloud (W)	Mixed-phase cloud (MP)	Dust-dominated aerosol (D)	Air pollutant (A)
Mar. 6 (Lanzhou)	-	-	-	-	15:00–17:00 1.0–2.0 km
Mar. 11 (Lanzhou)	19:30–20:00 6.0–7.0 km	-	21:00–22:00 2.5–3.0 km	18:00–20:00 0.5–1.5 km	10:00–12:00 2.5–2.8 km
Mar. 12 (Lanzhou)	-	13:00–15:00 1.8–2.0 km		-	-
Mar. 13 (Lanzhou)	17:00–19:00 8.5–9.5 km	-	-	-	15:00–17:00 1.0–2.0 km
Mar. 27 (Lanzhou)	-	-	3:00–4:00 3.5–4.0 km	6:00–9:00 0.5–2.0 km	-
Apr.11 (Linze)	-	12:30–15:00 2.8–3.5 km	-	-	-
Apr.13 (Linze)	18:00–20:20 7.0–8.5 km	-	-	-	-
Apr.14 (Linze)	-	-	2:00–3:00 3.2–4.0 km	0:00–4:00 0.5–1.0 km	-

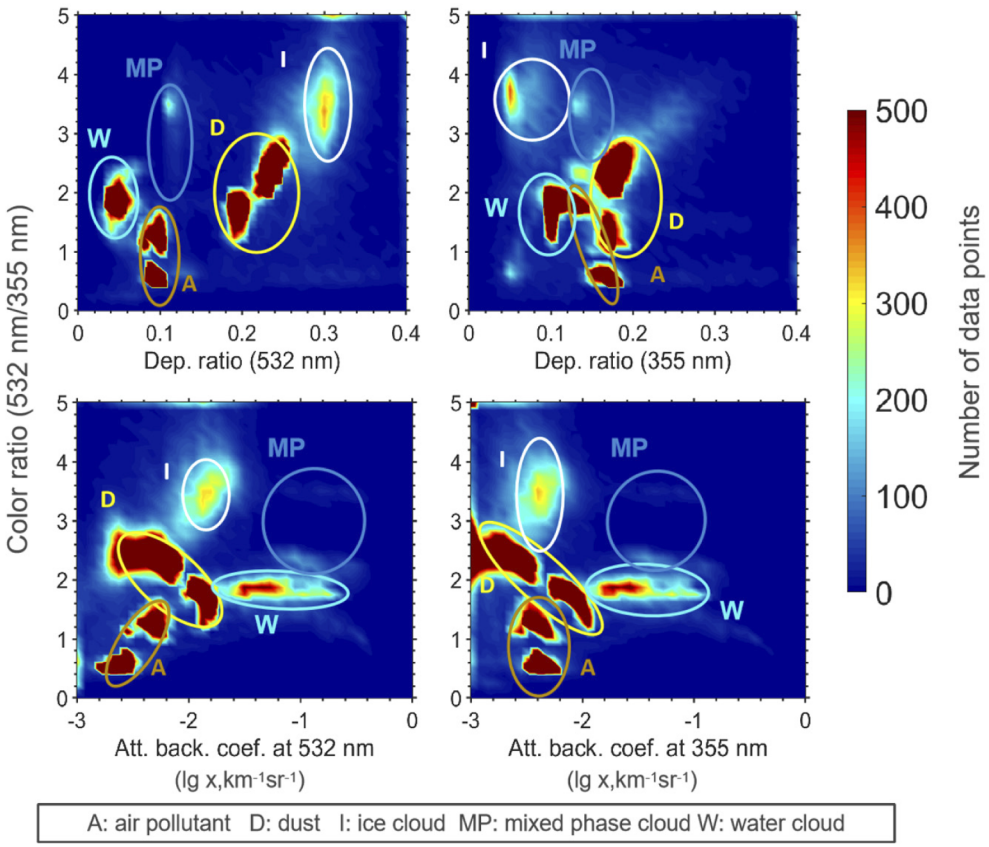

Fig. 4. Upper panel: relationships between the color ratio (532 nm/355 nm) and volume depolarization ratios at 532 nm and 355 nm. Lower panel: the relationships between the color ratio (532 nm/355 nm) and attenuated backscatter coefficient at 532 nm and 355 nm.

Optics EXPRESS

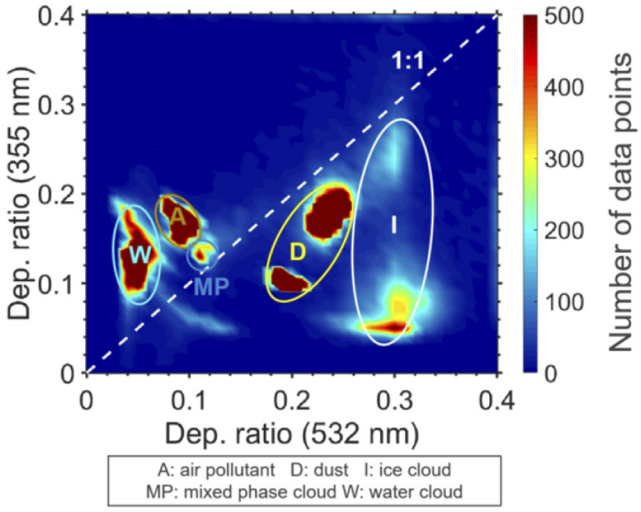

Fig. 5. Relationship between volume depolarization ratios at 532 nm and 355 nm for typical types of aerosols and clouds.

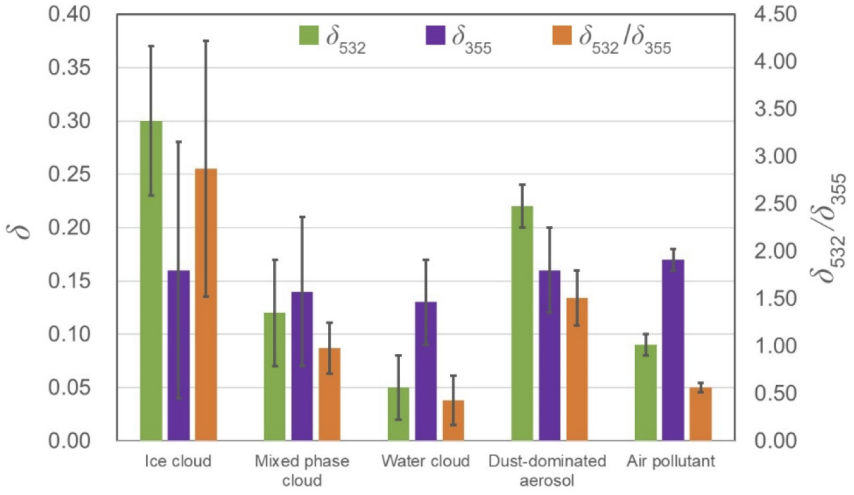

Fig. 6. Mean and standard deviation of volume depolarization ratios at 532 nm and 355 nm of typical aerosols and clouds.

Optics EXPRESS

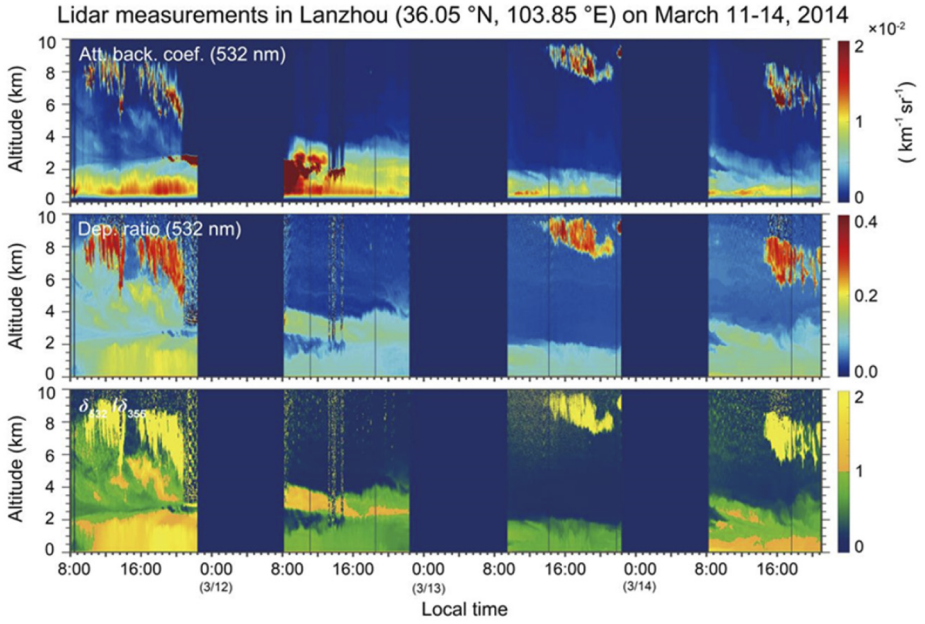

Fig. 7. Vertical structure of atmospheric aerosols and clouds from lidar observations in Lanzhou on March 11–14, 2014.

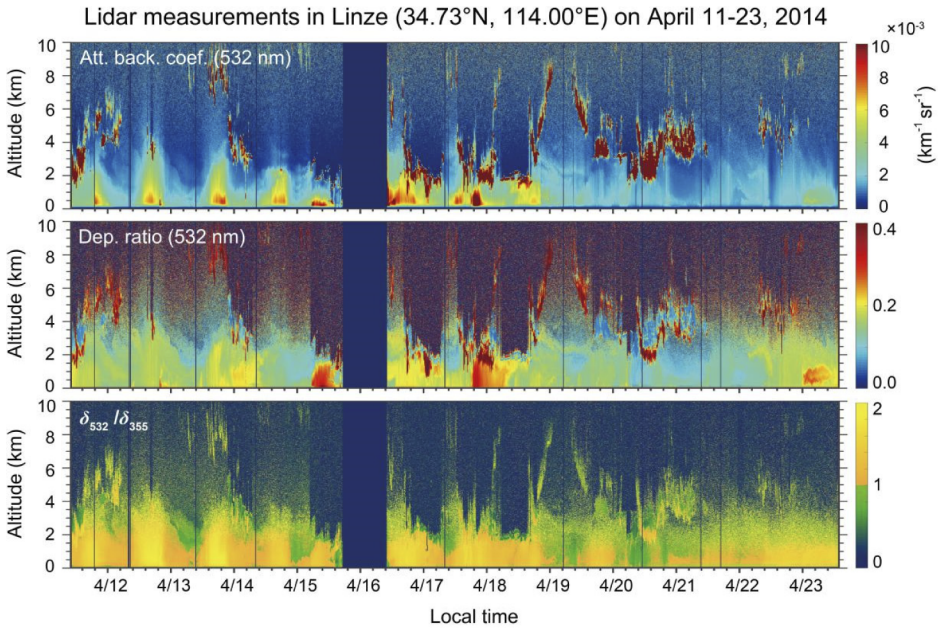

Fig. 8. Vertical structure of atmospheric aerosols and clouds from lidar observations in Linze on April 11–23, 2014.

Optics EXPRESS

than 0.5, but for ice clouds, these values are greater than 1.5. Using these results, we can clearly separate water clouds from ice clouds. In this study, mixed-phase clouds were detected during our observational period, leading to the identification of mixed-phase clouds being achieved, the

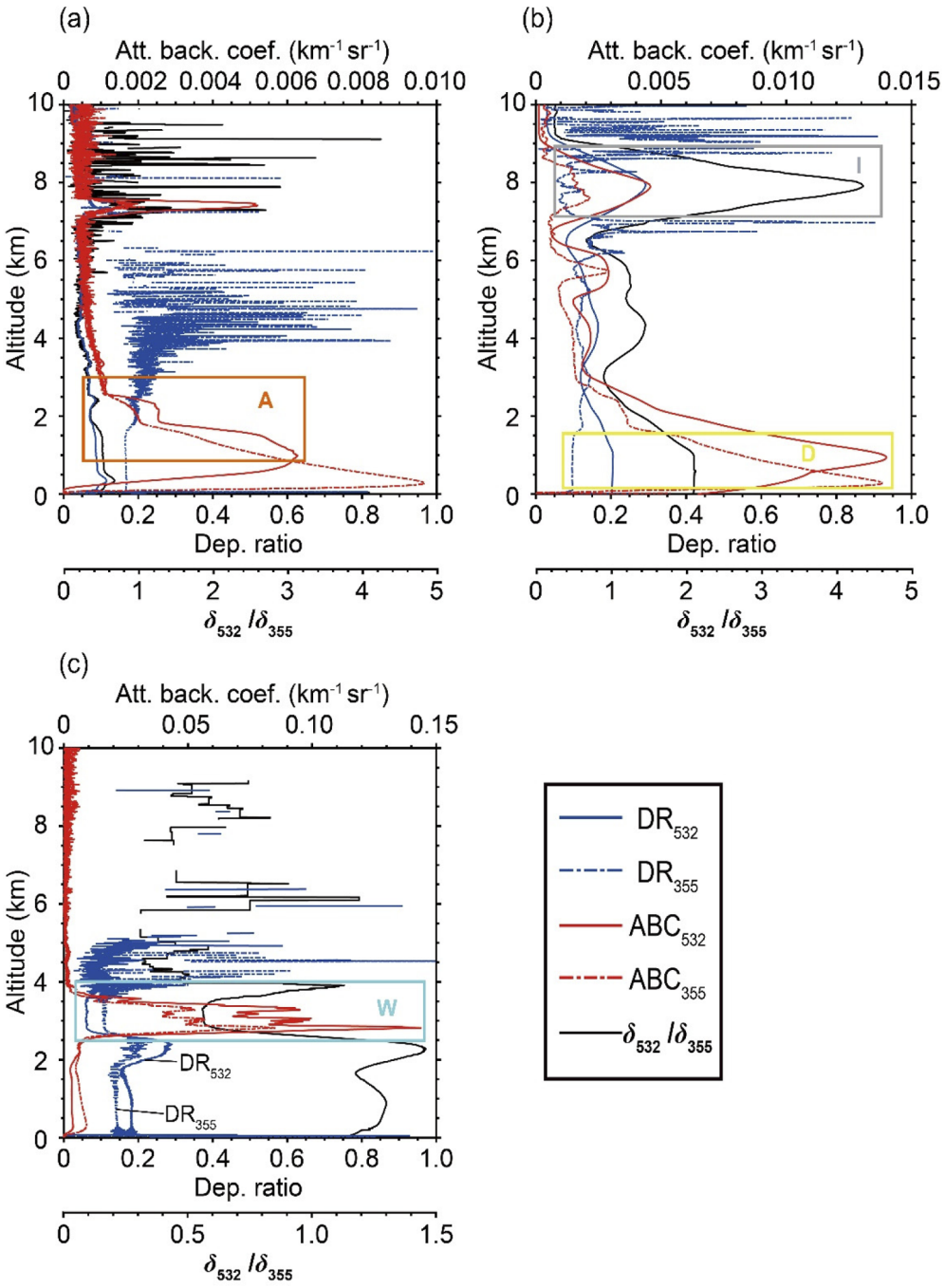

Fig. 9. Vertical profiles of lidar measurements. (a) Data are from Lanzhou at 14:00 on March 6, 2014; (b) Data are from Lanzhou at 18:00 on March 11, 2014; (c) Data are from Linze at 13:00 on April 11, 2014 (A: air pollutant; D: dust; W: water cloud; I: ice cloud).

Optics EXPRESS

ratio of VDRs for mixed-phase clouds are about 1.0. The value is consistent with the results of previous study [78]. Figure 9 shows the vertical profiles of three different time points, and the expression of the results is more intuitive. Finally, a method for accurately classifying typical types of aerosols and clouds from lidar measurements is proposed, and a flow chart of the proposed method is shown in Fig. 10. After correction of the lidar data, we first distinguished clouds from aerosols using a combination of the CR and ABC at 532 nm. Then, subtypes of clouds and aerosols are identified based on the ratio of VDRs at 532 nm and 355 nm.

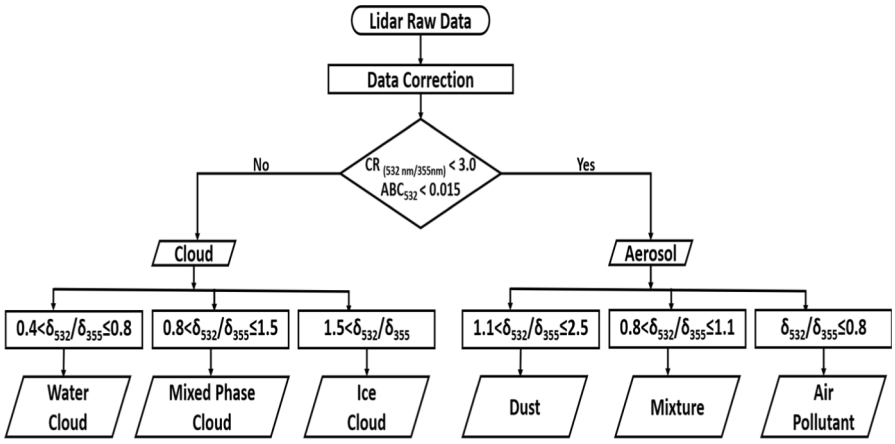

Fig. 10. Flow chart of the proposed method for classifying atmospheric aerosols and clouds from dual-polarization lidar measurements in this study.

We applied the proposed method to lidar measurements on March 6, and the vertical feature mask (VFM) of atmospheric aerosols and clouds could be obtained, as shown in Fig. 11. Ice cloud layers and water clouds on March 6 were successfully identified. For aerosols, we not only separated dust-dominated aerosols and air pollutants but also identified their mixture. The results of the classification using the proposed method have been roughly validated by weather records (dust event records), local in situ ground-based monitoring observation data and CALIPSO observation results.

Optics EXPRESS

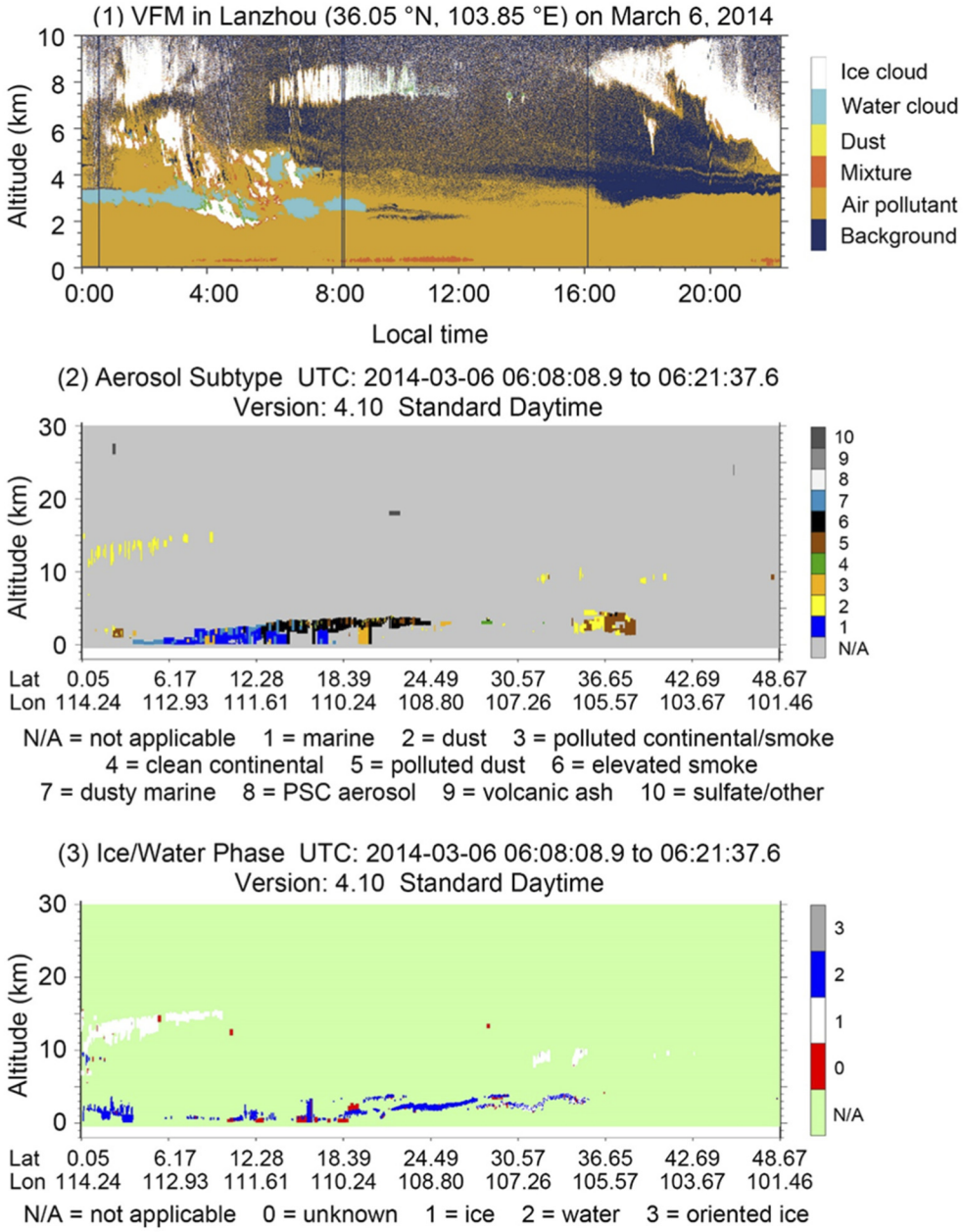

Fig. 11. (1) Vertical feature mask (VFM) of atmospheric aerosols and clouds identified using the proposed method from lidar measurements in Lanzhou on March 6, 2014. (2) and (3): VFM of atmospheric aerosols and clouds identified using CALIPSO.

Optics EXPRESS

4. Conclusions

In this study, we developed a ground-based dual-polarization lidar system that can simultaneously detect polarization measurements at wavelengths of 355 nm and 532 nm. The developed lidar was used to observe the vertical distribution of atmospheric aerosols and clouds over Northwest China in the spring 2014. Our results show that VDRs at 355 nm and 532 nm markedly differ for typical types of aerosols and clouds. For ice clouds and dust-dominated particles, the VDRs at 532 nm are larger than those at 355 nm. However, for water clouds and air pollutants, the VDRs at 532 nm are smaller than those at 355 nm. The ratio of VDRs at 532 nm and 355 nm are 2.87 ± 1.35 for ice clouds and $1.51 \pm 0.29$for dust-dominated particles, but these values are 0.43 ± 0.26 for water clouds and 0.56 ± 0.05 for air pollutants. Moreover, we proposed a simple reliable method for identifying atmospheric aerosols and clouds based on the spectral VDRs, CR and ABC at 532 nm. The proposed method first distinguishes clouds from aerosols using a combination of the CR and ABC at 532 nm. Then, subtypes of clouds and aerosols are identified based on the ratio of VDRs at 532 nm and 355 nm. The results showed that dual-polarization lidar measurements can remarkably improve the classification of atmospheric aerosols and clouds. It is proven that more information on atmospheric aerosols and clouds can be obtained from polarization lidar measurements at multiple wavelengths. This study encourages the laser remote sensing community to make lidar systems that can detect spectral VDRs for the study of aerosols and clouds in the atmosphere.

Funding. National Natural Science Foundation of China (41521004, 41627807, 41875029); Higher Education Discipline Innovation Project – 111 Project (B 13045).

Acknowledgments. Foundation of Key Laboratory for Semi-Arid Climate Change of the Ministry of Education in Lanzhou University.

Disclosures. The authors declare no conflicts of interest.

Data availability. Data underlying the results presented in this paper are not publicly available at this time but may be obtained from the authors upon reasonable request.

References

1. J. Huang, T. Wang, W. Wang, Z. Li, and H. Yan, "Climate effects of dust aerosols over East Asian arid and semiarid regions," J. Geophys. Res. Atmos. **119**(19), 11,398–11,416 (2014).
2. J. Bi, J. Huang, Z. Hu, B. N. Holben, and Z. Guo, "Investigating the aerosol optical and radiative characteristics of heavy haze episodes in Beijing during January of 2013," J. Geophys. Res. Atmos. **119**(16), 9884–9900 (2014).
3. Q. Fu, T. J. Thorsen, J. Su, J. M. Ge, and J. P. Huang, "Test of Mie-based single-scattering properties of non-spherical dust aerosols in radiative flux calculations," J. Quant. Spectrosc. Radiat. Transf. **110**(14-16), 1640–1653 (2009).
4. J. Bi, J. Huang, B. Holben, and G. Zhang, "Comparison of key absorption and optical properties between pure and transported anthropogenic dust over East and Central Asia," Atmos. Chem. Phys. **16**(24), 15501–15516 (2016).
5. T. Wang, Y. Han, J. Huang, M. Sun, B. Jian, Z. Huang, and H. Yan, "Climatology of dust-forced radiative heating over the Tibetan Plateau and its surroundings," J. Geophys. Res. Atmos. **125**, e2020JD032942 (2020).
6. V. Forster and P. and Ramaswamy, "Changes in Atmospheric Constituents and in Radiative Forcing, Climate Change 2007," Phys. Sci. Basis 129–234 (2007).
7. V. Ramanathan, P. J. Crutzen, J. T. Kiehl, and D. Rosenfeld, "Aerosols, Climate, and the Hydrological Cycle," Science **294**(5549), 2119–2124 (2001).
8. S. Liu, M. Chen, and Q. Zhuang, "Aerosol effects on global land surface energy fluxes during 2003-2010," Geophys. Res. Lett. **41**(22), 7875–7881 (2014).
9. U. Lohmann and J. Feichter, "Global indirect aerosol effects: a review," Atmos. Chem. Phys. **5**(3), 715–737 (2005).
10. W. Wang, J. Huang, P. Minnis, Y. Hu, J. Li, Z. Huang, J. K. Ayers, and T. Wang, "Dusty cloud properties and radiative forcing over dust source and downwind regions derived from A-Train data during the Pacific Dust Experiment," J. Geophys. Res. Atmos. **115**(24), 1–17 (2010).
11. H. Yan and T. Wang, "Ten Years of Aerosol Effects on Single-Layer Overcast Clouds over the US Southern Great Plains and the China Loess Plateau," Adv. Meteorol. **2020**, 6719160 (2020).
12. J. Li, J. Huang, K. Stamnes, T. Wang, Q. Lv, and H. Jin, "A global survey of cloud overlap based on CALIPSO and CloudSat measurements," Atmos. Chem. Phys. **15**(1), 519–536 (2015).
13. Z. Li, Y. Wang, J. Guo, C. Zhao, M. C. Cribb, X. Dong, J. Fan, D. Gong, J. Huang, M. Jiang, Y. Jiang, S. S. Lee, H. Li, J. Li, J. Liu, Y. Qian, D. Rosenfeld, S. Shan, Y. Sun, H. Wang, J. Xin, X. Yan, X. Yang, X. qun Yang, F. Zhang, and Y. Zheng, "East Asian Study of Tropospheric Aerosols and their Impact on Regional Clouds, Precipitation, and Climate (EAST-AIRCPC)," J. Geophys. Res. Atmos. **124**(23), 13026–13054 (2019).

Optics EXPRESS

14. J. L. Brenguier, H. Pawlowska, L. Schüller, R. Preusker, J. Fischer, and Y. Fouquart, "Radiative properties of boundary layer clouds: Droplet effective radius versus number concentration," J. Atmos. Sci. **57**(6), 803–821 (2000).
15. E. Berry and G. G. Mace, "Cloud properties and radiative effects of the Asian summer monsoon derived from A-Train data," J. Geophys. Res. Atmos. **119**(15), 9492–9508 (2014).
16. T. J. Garrett and C. Zhao, "Increased Arctic cloud longwave emissivity associated with pollution from mid-latitudes," Nature **440**(7085), 787–789 (2006).
17. S. Twomey, "The Influence of Pollution on the Shortwave Albedo of Clouds," J. Atmos. Sci. **34**(7), 1149–1152 (1977).
18. S. Sherwood and Q. Fu, "A drier future?" Science. **343**(6172), 737–739 (2014).
19. S. Lolli, W. Y. Khor, M. Z. Matjafri, and H. S. Lim, "Monsoon season quantitative assessment of biomass burning clear-sky aerosol radiative effect at surface by ground-based lidar observations in pulau pinang, Malaysia in 2014," Remote Sens. **11**(22), 2660 (2019).
20. T. Zhang, H. Che, Z. Gong, Y. Wang, J. Wang, Y. Yang, K. Gui, and B. Guo, "The two-way feedback effect between aerosol pollution and planetary boundary layer structure on the explosive rise of PM2.5 after the "Ten Statements of Atmosphere" in Beijing," Sci. Total Environ. **709**, 136259 (2020).
21. Y. S. Koo, H. Y. Yun, D. R. Choi, J. S. Han, J. B. Lee, and Y. J. Lim, "An analysis of chemical and meteorological characteristics of haze events in the Seoul metropolitan area during January 12–18, 2013," Atmos. Environ. **178**(2018), 87–100 (2018).
22. T. Sun, H. Che, B. Qi, Y. Wang, Y. Dong, X. Xia, H. Wang, K. Gui, Y. Zheng, H. Zhao, Q. Ma, R. Du, and X. Zhang, "Aerosol optical characteristics and their vertical distributions under enhanced haze pollution events: Effect of the regional transport of different aerosol types over eastern China," Atmos. Chem. Phys. **18**(4), 2949–2971 (2018).
23. J. Chen, Z. Li, M. Lv, Y. Wang, W. Wang, Y. Zhang, H. Wang, X. Yan, Y. Sun, and M. Cribb, "Aerosol hygroscopic growth, contributing factors, and impact on haze events in a severely polluted region in northern China," Atmos. Chem. Phys. **19**(2), 1327–1342 (2019).
24. J. R. Campbell, D. L. Hlavka, E. J. Welton, C. J. Flynn, D. D. Turner, J. D. Spinhirne, S. Stanley, and I. H. Hwang, "Full-time, eye-safe cloud and aerosol lidar observation at atmospheric radiation measurement program sites: Instruments and data processing," J. Atmos. Ocean. Technol. **19**(4), 431–442 (2002).
25. D. Müller, K. H. Lee, J. Gasteiger, M. Tesche, B. Weinzierl, K. Kandler, T. Müller, C. Toledano, S. Otto, D. Althausen, and A. Ansmann, "Comparison of optical and microphysical properties of pure Saharan mineral dust observed with AERONET Sun photometer, Raman lidar, and in situ instruments during SAMUM 2006," J. Geophys. Res. Atmos. **117**(7), (2012).
26. N. Sugimoto, I. Matsui, A. Shimizu, I. Uno, K. Asai, T. Endoh, and T. Nakajima, "Observation of dust and anthropogenic aerosol plumes in the Northwest Pacific with a two-wavelength polarization lidar on board the research vessel Mirai," Geophys. Res. Lett. **29**(19), 7-1–7-4 (2002).
27. N. Sugimoto and Z. Huang, "Lidar methods for observing mineral dust," J. Meteorol. Res. **28**(2), 173–184 (2014).
28. J. Huang, P. Minnis, B. Chen, Z. Huang, Z. Liu, Q. Zhao, Y. Yi, and J. K. Ayers, "Long-range transport and vertical structure of Asian dust from CALIPSO and surface measurements during PACDEX," J. Geophys. Res. Atmos. **113**(23), 1–13 (2008).
29. J. P. Huang, J. J. Liu, B. Chen, and S. L. Nasiri, "Detection of anthropogenic dust using CALIPSO lidar measurements," Atmos. Chem. Phys. **15**(20), 11653–11665 (2015).
30. T. Nishizawa, N. Sugimoto, I. Matsui, A. Shimizu, Y. Hara, U. Itsushi, K. Yasunaga, R. Kudo, and S. W. Kim, "Ground-based network observation using Mie–Raman lidars and multi-wavelength Raman lidars and algorithm to retrieve distributions of aerosol components," J. Quant. Spectrosc. Radiat. Transf. **188**, 79–93 (2017).
31. J. Reichardt, U. Wandinger, V. Klein, I. Mattis, B. Hilber, and R. Begbie, "RAMSES: German meteorological service autonomous Raman lidar for water vapor, temperature, aerosol, and cloud measurements," Appl. Opt. **51**(34), 8111–8131 (2012).
32. J. M. Intrieri, M. D. Shupe, T. Uttal, and B. J. McCarty, "An annual cycle of Arctic cloud characteristics observed by radar and lidar at SHEBA," J. Geophys. Res. Ocean. **107**(10), SHE 5-1–SHE 5-15 (2002).
33. J. Li, B. Jian, J. Huang, Y. Hu, C. Zhao, K. Kawamoto, S. Liao, and M. Wu, "Long-term variation of cloud droplet number concentrations from space-based Lidar," Remote Sens. Environ. **213**(1), 144–161 (2018).
34. J. E. Yorks, D. L. Hlavka, W. D. Hart, and M. J. Mcgill, "Statistics of cloud optical properties from airborne lidar measurements," J. Atmos. Ocean. Technol. **28**(7), 869–883 (2011).
35. A. Ansmann, F. Wagner, D. Müller, D. Althausen, A. Herber, W. Von Hoyningen-Huene, and U. Wandinger, "European pollution outbreaks during ACE 2: Optical particle properties inferred from multiwavelength lidar and star-Sun photometry," J. Geophys. Res. Atmos. **107**(15), AAC 8-1–AAC 8-14 (2002).
36. M. Tesche, A. Ansmann, D. Müller, D. Althausen, I. Mattis, B. Heese, V. Freudenthaler, M. Wiegner, M. Esselborn, G. Pisani, and P. Knippertz, "Vertical profiling of Saharan dust with Raman lidars and airborne HSRL in southern Morocco during SAMUM," Tellus, Ser. B Chem. Phys. Meteorol. **61**(1), 144–164 (2009).
37. T. Zhou, H. Xie, J. Bi, Z. Huang, J. Huang, J. Shi, B. Zhang, and W. Zhang, "Lidar measurements of dust aerosols during three field campaigns in 2010, 2011 and 2012 over northwestern China," Atmosphere (Basel). **9**(5), 173 (2018).
38. L. Fang, S. Wang, T. Yu, X. Gu, X. Zhang, W. Wang, and S. Ren, "Changes in aerosol optical and micro-physical properties over Northeast Asia from a severe dust storm in April 2014," Remote Sens. **8**(5), 394 (2016).

Optics EXPRESS

39. R. J. Park, M. J. Kim, J. I. Jeong, D. Youn, and S. Kim, "A contribution of brown carbon aerosol to the aerosol light absorption and its radiative forcing in East Asia," Atmos. Environ. **44**(11), 1414–1421 (2010).
40. Z. Huang, J. Huang, J. Bi, G. Wang, W. Wang, Q. Fu, Z. Li, S.-C. Tsay, and J. Shi, "Dust aerosol vertical structure measurements using three MPL lidars during 2008 China-U.S. joint dust field experiment," J. Geophys. Res. **115**(13), 1299–1303 (2010).
41. J. Bi, J. Huang, J. Shi, Z. Hu, T. Zhou, G. Zhang, Z. Huang, X. Wang, and H. Jin, "Measurement of scattering and absorption properties of dust aerosol in a Gobi farmland region of northwestern China - A potential anthropogenic influence," Atmos. Chem. Phys. **17**(12), 7775–7792 (2017).
42. Z. Huang, J. Huang, T. Hayasaka, S. Wang, T. Zhou, and H. Jin, "Short-cut transport path for Asian dust directly to the Arctic: A case study," Environ. Res. Lett. **10**(11), 114018 (2015).
43. Z. Huang, J. B. Nee, C. W. Chiang, S. Zhang, H. Jin, W. Wang, and T. Zhou, "Real-time observations of dust-cloud interactions based on polarization and Raman lidar measurements," Remote Sens. **10**(7), 1–14 (2018).
44. T. Wang, Y. Chen, Z. Gan, Y. Han, J. Li, and J. Huang, "Assessment of dominating aerosol properties and their long-term trend in the Pan-Third Pole region: A study with 10-year multi-sensor measurements," Atmos. Environ. **239**, 117738 (2020).
45. Q. Hu, H. Wang, P. Goloub, Z. Li, I. Veselovskii, T. Podvin, K. Li, and M. Korenskiy, "The characterization of Taklamakan dust properties using a multiwavelength Raman polarization lidar in Kashi, China," Atmos. Chem. Phys. **20**(22), 13817–13834 (2020).
46. N. Sugimoto, Z. Huang, T. Nishizawa, I. Matsui, and B. Tatarov, "Fluorescence from atmospheric aerosols observed with a multi-channel lidar spectrometer," Opt. Express **20**(19), 20800 (2012).
47. Z. Liu, A. Omar, M. Vaughan, J. Hair, C. Kittaka, Y. Hu, K. Powell, C. Trepte, D. Winker, C. Hostetler, R. Ferrare, and R. Pierce, "CALIPSO lidar observations of the optical properties of Saharan dust: A case study of long-range transport," J. Geophys. Res. Atmos. **113**, D07207 (2008).
48. A. Kumar, N. Singh, R. Anshumali, and Solanki, "Evaluation and utilization of MODIS and CALIPSO aerosol retrievals over a complex terrain in Himalaya," Remote Sens. Environ. **206**(2018), 139–155 (2018).
49. J. Huang, P. Minnis, Y. Yi, Q. Tang, X. Wang, Y. Hu, Z. Liu, K. Ayers, C. Trepte, and D. Winker, "Summer dust aerosols detected from CALIPSO over the Tibetan Plateau," Geophys. Res. Lett. **34**(18), L18805 (2007).
50. A. Devasthale, M. Tjernström, and A. H. Omar, ""The vertical distribution of thin features over the Arctic analysed from CALIPSO observations: Part II: Aerosols," Tellus," Ser. B Chem. Phys. Meteorol. **63**(1), 86–95 (2011).
51. F. Cairo, G. Di Donfrancesco, A. Adriani, L. Pulvirenti, and F. Fierli, "Comparison of various linear depolarization parameters measured by lidar," Appl. Opt. **38**(21), 4425 (1999).
52. J. Hofer, D. Althausen, S. F. Abdullaev, A. N. Makhmudov, B. I. Nazarov, G. Schettler, R. Engelmann, H. Baars, K. W. Fomba, K. Müller, B. Heinold, K. Kandler, and A. Ansmann, "Long-term profiling of mineral dust and pollution aerosol with multiwavelength polarization Raman lidar at the Central Asian site of Dushanbe, Tajikistan: Case studies," Atmos. Chem. Phys. **17**(23), 14559–14577 (2017).
53. D. Mamali, E. Marinou, J. Sciare, M. Pikridas, P. Kokkalis, M. Kottas, I. Binietoglou, A. Tsekeri, C. Keleshis, R. Engelmann, H. Baars, A. Ansmann, V. Amiridis, H. Russchenberg, and G. Biskos, "Vertical profiles of aerosol mass concentration derived by unmanned airborne in situ and remote sensing instruments during dust events," Atmos. Meas. Tech. **11**(5), 2897–2910 (2018).
54. C. Böckmann, U. Wandinger, A. Ansmann, J. Bo, V. Amiridis, A. Boselli, A. Delaval, F. De Tomasi, M. Frioud, I. V. Grigorov, A. Hågård, M. Horvat, M. Iarlori, L. Komguem, S. Kreipl, G. Larcheve, V. Matthias, A. Papayannis, G. Pappalardo, F. Rocadenbosch, J. Schneider, V. Shcherbakov, and C. Universitario, "Aerosol lidar intercomparison in the framework of the EARLINET project. 2. Aerosol backscatter algorithms," Appl. Opt. **43**(4), 977–989 (2004).
55. A. Ansmann, U. Wandinger, M. Riebesell, C. Weitkamp, and W. Michaelis, "Independent measurement of extinction and backscatter profiles in cirrus clouds by using a combined Raman elastic-backscatter lidar," Appl. Opt. **31**(33), 7113 (1992).
56. M. McGill, D. Hlavka, W. Hart, V. S. Scott, J. Spinhirne, and B. Schmid, "Cloud Physics Lidar: instrument description and initial measurement results," Appl. Opt. **41**(18), 3725 (2002).
57. N. Papagiannopoulos, L. Mona, A. Amodeo, G. D'Amico, P. Gumà Claramunt, G. Pappalardo, L. Alados-Arboledas, J. Luís Guerrero-Rascado, V. Amiridis, P. Kokkalis, A. Apituley, H. Baars, A. Schwarz, U. Wandinger, I. Binietoglou, D. Nicolae, D. Bortoli, A. Comerón, A. Rodríguez-Gómez, M. Sicard, A. Papayannis, and M. Wiegner, "An automatic observation-based aerosol typing method for EARLINET," Atmos. Chem. Phys. **18**(21), 15879–15901 (2018).
58. K. Ohneiser, A. Ansmann, H. Baars, P. Seifert, B. Barja, C. Jimenez, M. Radenz, A. Teisseire, A. Floutsi, M. Haarig, R. Engelmann, F. Zamorano, J. Bühl, and U. Wandinger, "Smoke of extreme Australian bushfires observed in the stratosphere over Punta Arenas, Chile, in January 2020: optical thickness, lidar ratios, and depolarization ratios at 355 and 532 nm," Atmos. Chem. Phys. Discuss. (January), 1–16 (2020).
59. S. P. Burton, R. A. Ferrare, C. A. Hostetler, J. W. Hair, R. R. Rogers, M. D. Obland, C. F. Butler, A. L. Cook, D. B. Harper, and K. D. Froyd, "Aerosol classification using airborne High Spectral Resolution Lidar measurements-methodology and examples," Atmos. Meas. Tech. **5**(1), 73–98 (2012).
60. L. Mona, A. Amodeo, G. D'Amico, A. Giunta, F. Madonna, and G. Pappalardo, "Multi-wavelength Raman lidar observations of the Eyjafjallajökull volcanic cloud over Potenza, southern Italy," Atmos. Chem. Phys. **12**(4), 2229–2244 (2012).

Optics EXPRESS

61. D. Müller, K. Franke, F. Wagner, D. Althausen, A. Ansmann, and J. Heintzenberg, "Vertical profiling of optical and physical particle properties over the tropical Indian Ocean with six-wavelength lidar 1. Seasonal cycle," J. Geophys. Res. Atmos. **106**(D22), 28567–28575 (2001).
62. V. Noel and H. Chepfer, "A global view of horizontally oriented crystals in ice clouds from Cloud-Aerosol Lidar and Infrared Pathfinder Satellite Observation (CALIPSO)," J. Geophys. Res. **115**(D4), D00H23 (2010).
63. J. M. Intrieri, G. L. Stephens, W. L. Eberhard, and T. Uttal, "A method for determining cirrus cloud particle sizes using lidar and radar backscatter technique," J. Appl. Meteorol. **32**(6), 1074–1082 (1993).
64. H.-M. Cho, P. Yang, G. W. Kattawar, S. L. Nasiri, Y. Hu, P. Minnis, C. Trepte, and D. Winker, "Depolarization ratio and attenuated backscatter for nine cloud types: analyses based on collocated CALIPSO lidar and MODIS measurements," Opt. Express **16**(6), 3931–3948 (2008).
65. K. Sassen, "The polarization lidar technique for cloud research: a review and current assessment," Bull. - Am. Meteorol. Soc. **72**(12), 1848–1866 (1991).
66. Z. Liu, M. A. Vaughan, D. M. Winker, C. A. Hostetler, L. R. Poole, D. Hlavka, W. Hart, and M. McGill, "Use of probability distribution functions for discriminating between clouds and aerosol in lidar backscatter data," J. Geophys. Res. D Atmos. **109**(15), 1–13 (2004).
67. Z. Liu, M. Vaughan, D. Winker, C. Kittaka, B. Getzewich, R. Kuehn, A. Omar, K. Powell, C. Trepte, and C. Hostetler, "The CALIPSO lidar cloud and aerosol discrimination: Version 2 algorithm and initial assessment of performance," J. Atmos. Ocean. Technol. **26**(7), 1198–1213 (2009).
68. T. Zhou, J. Huang, Z. Huang, J. Liu, W. Wang, and L. Lin, "The depolarization–attenuated backscatter relationship for dust plumes," Opt. Express **21**(13), 15195 (2013).
69. Z. Wang and K. Sassen, "Cloud type and macrophysical property retrieval using multiple remote sensors," J. Appl. Meteorol. **40**(10), 1665–1682 (2001).
70. C. Zhao, Y. Wang, Q. Wang, Z. Li, Z. Wang, and D. Liu, "A new cloud and aerosol layer detection method based on micropulse lidar measurements," J. Geophys. Res. Atmos. **119**(11), 6788–6802 (2014).
71. I. Veselovskii, A. Kolgotin, V. Griaznov, D. Mu, K. Franke, and D. N. Whiteman, "Inversion of multiwavelength Raman lidar data for retrieval of bimodal aerosol size distribution," Appl. Opt. **43**(5), 1180–1195 (2004).
72. S. Groß, M. Esselborn, F. Abicht, M. Wirth, A. Fix, and A. Minikin, "Airborne high spectral resolution lidar observation of pollution aerosol during EUCAARI-LONGREX," Atmos. Chem. Phys. **13**(5), 2435–2444 (2013).
73. A. A. Floutsi, H. Baars, M. Radenz, M. Haarig, Z. Yin, P. Seifert, C. Jimenez, A. Ansmann, R. Engelmann, B. Barja, F. Zamorano, and U. Wandinger, "Advection of biomass burning aerosols towards the southern hemispheric mid-latitude station of punta arenas as observed with multiwavelength polarization raman lidar," Remote Sens. **13**(1), 138 (2021).
74. S. P. Burton, M. A. Vaughan, R. A. Ferrare, and C. A. Hostetler, "Separating mixtures of aerosol types in airborne High Spectral Resolution Lidar data," Atmos. Meas. Tech. **7**(2), 419–436 (2014).
75. S. P. Burton, J. W. Hair, M. Kahnert, R. A. Ferrare, C. A. Hostetler, A. L. Cook, D. B. Harper, T. A. Berkoff, S. T. Seaman, J. E. Collins, M. A. Fenn, and R. R. Rogers, "Observations of the spectral dependence of linear particle depolarization ratio of aerosols using NASA Langley airborne High Spectral Resolution Lidar," Atmos. Chem. Phys. **15**(23), 13453–13473 (2015).
76. Z. Huang, S. Qi, T. Zhou, Q. Dong, X. Ma, S. Zhang, J. Bi, and J. Shi, "Investigation of aerosol absorption with dual-polarization lidar observations," Opt. Express **28**(5), 7028 (2020).
77. M. I. Mishchenko, J. M. Dlugach, and L. Liu, "Linear depolarization of lidar returns by aged smoke particles," Appl. Opt. **55**(35), 9968 (2016).
78. I. Veselovskii, P. Goloub, T. Podvin, D. Tanre, A. Ansmann, M. Korenskiy, A. Borovoi, Q. Hu, and D. N. Whiteman, "Spectral dependence of backscattering coefficient of mixed phase clouds over West Africa measured with two-wavelength Raman polarization lidar: Features attributed to ice-crystals corner reflection," J. Quant. Spectrosc. Radiat. Transf. **202**, 74–80 (2017).